



## Kinematics of décollement folding in the Lost River Range, Idaho

DAVID J. ANASTASIO

Department of Earth and Environmental Sciences, Lehigh University, Bethlehem, PA 18015-3188, U.S.A.

DONALD M. FISHER

Department of Geosciences, Pennsylvania State University, University Park, PA 16802, U.S.A.

THERESA A. MESSINA\*

Department of Earth and Environmental Sciences, Lehigh University, Bethlehem, PA 18015-3188, U.S.A.

and

JAMES E. HOLL†

Department of Earth and Environmental Sciences, Lehigh University, Bethlehem, PA 18015-3188, U.S.A.

(Received 26 March 1996; accepted in revised form 19 November 1996)

**Abstract**—Décollement folding of massive (> 2 m thick) carbonate beds of the Scott Peak Formation, within the Willow Creek anticline, northern Lost River Range, Idaho was associated with the development of thin (< 0.25 m), widely-spaced deformation zones. Incremental strain histories determined from fibrous overgrowths in strain fringes from the deformation zones provide a basis for kinematic analysis of the anticline. Plane strain is indicated by coaxial up-dip extension on cleavage (*XY*) planes and a lack of extension in the *Y* direction. In *XZ* sections, coaxial incremental strain histories characterize fold hinges and document pinned hinges during folding. The sense of rotation on opposing limbs indicates that the fiber curvature records primarily the spin of layers through fixed, moderately steep ( $66^\circ \pm 12^\circ$  ( $1\sigma$ )), diverging extension directions. The magnitude of the external rotation for each sample is typically less than the bedding dip, suggesting that the external rotation also includes a component of internal rotation related to layer-parallel shear toward the upper flat panel or the hinge pin line. The magnitude of this internal rotation varies within and between layers. © 1997 Elsevier Science Ltd

### INTRODUCTION

The long recognized geometric association between folding and faulting (Heim, 1921) has led to numerous quantitative fold–fault models based primarily on structural geometry but from which kinematics and mechanics are often inferred (Suppe, 1983; Jamison, 1992). Fault-related folds within thrust belts are commonly defined in terms of the geometric relationship between the fault and the fold. For example, fault-bend folds are observed above bends in the trailing edge of the thrust sheet (Rich, 1934; Suppe, 1983), fault-propagation folds occupy the leading edges of thrust sheets (Suppe and Medwedeff, 1990), and décollement folds are observed above bedding-parallel faults (Namson, 1981; Boyer, 1986; Jamison, 1987; Dahlstrom, 1990; Epard and Groshong, 1993; Homza and Wallace, 1995). Classification of fault-related

folding based solely on geometry may be misleading, because the terms used to describe fault-related folds in some cases carry kinematic implications that may not be valid. In dynamically-scaled analogue models, décollement folds produced by buckling can evolve into folds that are indistinguishable from fault-bend folds (Dixon and Liu, 1992). Propagation of a ramp through a décollement fold produces a geometry similar to fault-propagation folds and breaching of the fold leads to a fault-bend fold geometry (Dixon and Liu, 1992). The prevalence of footwall synclines in many foreland provinces also supports décollement folding prior to ramp propagation and subsequent fault-bend folding of the hanging wall (Cooper and Trayner, 1986).

Balanced geometric models of fault-related folds have been successful in predicting subsurface structural geometries. However, geometry alone does not uniquely constrain finite strain distributions, fold kinematics, or mechanics (Fig. 1). Forward geometric models of fault-propagation and fault-bend folds predict migration of material through spatially fixed axial surfaces (Suppe, 1983; Jamison, 1987; Suppe and Medwedeff, 1990). In a

\*Present address: Amerada Hess Company, 1 Hess Plaza, Woodbridge, NJ 07095, U.S.A.

† Present address: Exxon Production Research Company, Houston, TX 77252-2189, U.S.A.

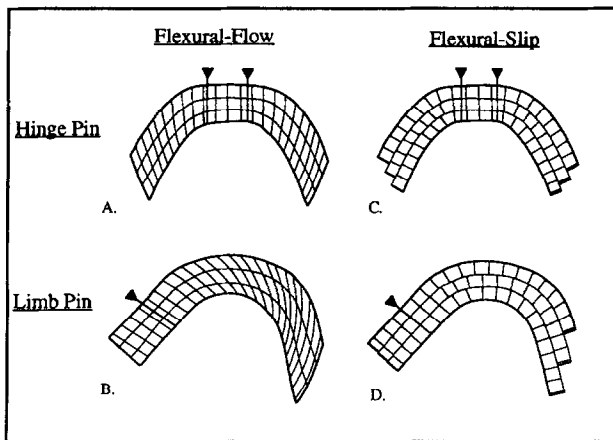


Fig. 1. Variations in boundary conditions (fold shape and pin position) and folding mechanism (flexural-slip versus flexural-flow) affect strain histories and the distribution of finite strain. Flexural-flow strain patterns from paper stack experiments (130 layers), flexural-slip patterns are theoretical.

few emergent leading edge folds, analysis of growth stratal geometries have been used to infer self-similar fold growth and migrating hinges (Suppe *et al.*, 1992, 1997; Zapata and Allmendinger, 1996). In contrast, some finite and incremental strain studies (Fischer *et al.*, 1992; Fisher and Anastasio, 1994; Hedlund *et al.*, 1994) support initial fixed hinge buckling prior to fault-bend folding in penetratively deformed, fault-related folds.

For décollement folds, a variety of kinematic possibilities exist (Poblet and McClay, 1996) based on (1) the position of pin lines, (2) fixed (De Sitter, 1956) versus migrating (Dahlstrom, 1990) axial surfaces, and (3) variable (Homza and Wallace, 1995) versus fixed (Namson, 1981; Epard and Groshong, 1993) décollement depth. Backstripping and unfolding approaches have the potential to distinguish between fixed and migrating axial surfaces for synsedimentary near-surface décollement folds (Holl and Anastasio, 1993; Poblet and Hardy, 1995; Hardy and Poblet, 1994). However, analysis of growth strata requires knowledge of surface displacements and numerous assumptions about surficial processes. Another approach to the evaluation of fold kinematics is incremental and finite strain analysis which allow for assessment of the distribution, magnitude, and temporal variation of the displacements throughout a fault-related fold. In this study, we present incremental strain data from fibrous overgrowths in strain fringes to constrain the kinematics of large-scale décollement folding in the northern Lost River Range, Idaho.

#### FOLDING IN THE NORTHERN LOST RIVER RANGE, IDAHO

The Lost River Range is one of a series of NW–SE trending mountain ranges in Idaho, east of the Idaho

batholith, west of the Sevier thrust front, and north of the Snake River Plain. The range exposes the Lost River Range–Arco Hills thrust sheet which has been folded into a regional synclinorium comprised of variably sized disharmonic folds (Fig. 2; Ross, 1947; Mapel *et al.*, 1965; Messina, 1993). The stratigraphy of the thrust sheet includes Antler flysch (McGowan Creek Formation), overlain by a late Paleozoic westward thickening carbonate platform (Mapel *et al.*, 1965). The McGowan Creek Formation is an eastward thinning wedge of predominantly thin-bedded siltstone and argillite which had a depositional thickness of 150–60 m across the range (Sandberg, 1975). The late Paleozoic platform stratigraphy is ~1650 m thick in the northern Lost River Range (Mapel *et al.*, 1965).

Regional stratigraphic reconstructions and balanced and restored cross-sections of the Idaho–Wyoming–Montana thrust belt, suggest that compressional deformation within the Lost River Range occurred at a depth of ~10 km (Mamet *et al.*, 1971; Allmendinger, 1990). Illite crystallinity analysis of the Scott Peak Formation (Mississippian limestone) within the Lost River Range indicates peak metamorphic temperatures of 220°C during Cretaceous deformation (Hedlund *et al.*, 1994).

Regional folds within the upper Paleozoic carbonates of the Arco Hills–Lost River Range thrust sheet have parallel, kink geometries, are upright, and plunge shallowly (<20°) to either the northwest or southeast (Ross, 1947; Mapel *et al.*, 1965; Janecke and Wilson, 1992; Messina, 1993). Line length restoration of the Scott Peak Formation within the thrust sheet along a 12 km section through Christian Gultch (Fig. 2) yields a shortening of 2.64 km or 22%. Most folds within the thrust sheet are décollement folds although fault-bend (Hedlund *et al.*, 1994) and fault-propagation fold geometries (Fisher and Anastasio, 1994) also occur. Depth-to-décollement calculations (Chamberlain, 1910; Dahlstrom, 1969, 1990; Epard and Groshong, 1993; Homza and Wallace, 1995) predict a regional décollement near the base of the McGowan Creek Formation. Folds within the upper Paleozoic carbonate section decrease in amplitude eastward as the McGowan Creek Formation thins. Folds within the McGowan Creek Formation decrease in amplitude down section towards the regional décollement (Messina, 1993).

Subsequent to the Sevier orogeny, the northern Lost River Range experienced variable amounts of vertical axis rotation and tilt as a result of middle Eocene extension on the Lemhi and Donkey Hills faults (Janecke *et al.*, 1991; Rodgers and Janecke, 1992; Anders *et al.*, 1993). Willow Creek anticline is a large-scale décollement fold located in the hanging wall of the shallowly west-dipping Donkey Hills extensional fault and in the foot-wall of the steep (75°) Lost River extensional fault, along the western side of the Lost River Range. Orientation analysis of bedding, cleavage, and incremental extension directions from both fold limbs with respect to geographic horizontal preclude any post-Sevier tilting at

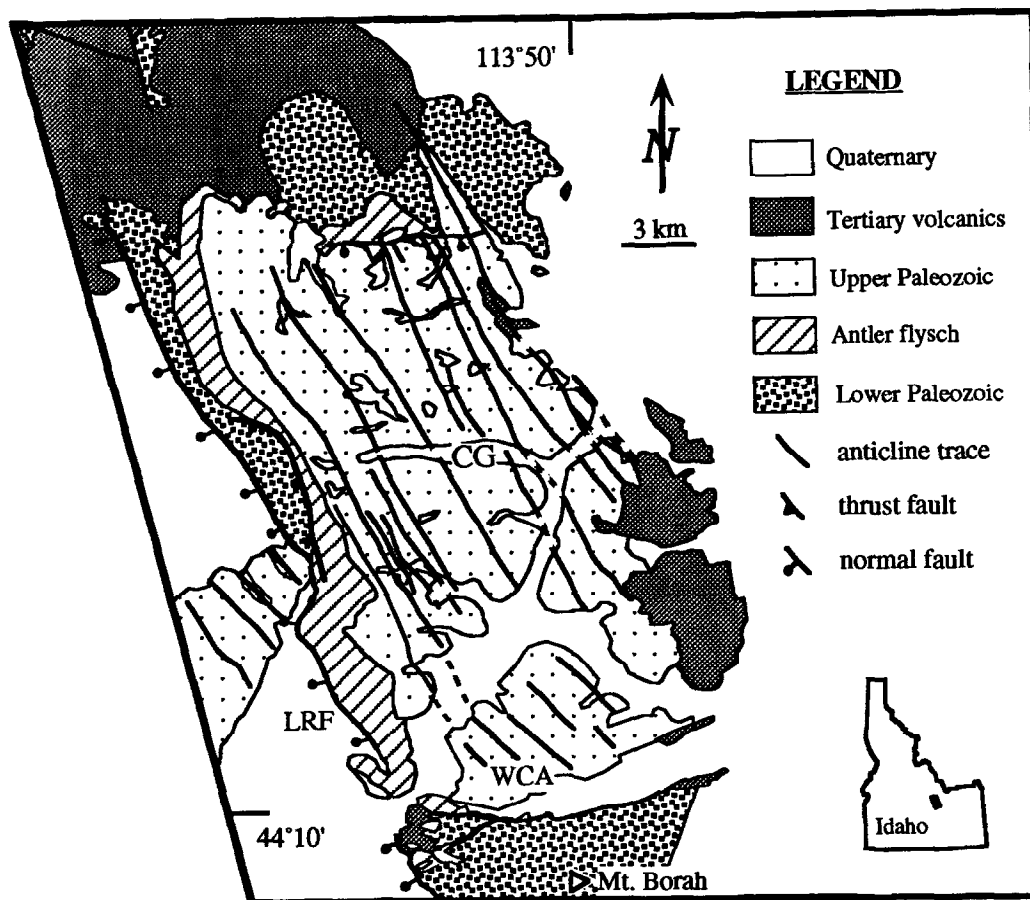


Fig. 2. Generalized geologic map of northern Lost River Range in eastern Idaho (in part after Ross, 1947; Mapel *et al.*, 1965 and Janecke and Wilson, 1992). Only second- and third-order anticlinal axial traces within the upper Palaeozoic section are shown. WCA: Willow Creek anticline, LRF: Lost River fault, CG: Christian Gulch.

Willow Creek, but the anticline likely underwent a rigid, counterclockwise, vertical axis rotation subsequent to Cretaceous fold formation (Janecke *et al.*, 1991). This post-folding, rigid rotation does not affect our analysis of fold kinematics as all reference frames (bedding, cleavage, and horizontal) were rotated uniformly.

#### *Willow Creek anticline*

An anticline located at the head of Willow Creek was chosen for kinematic analysis because of its well-exposed geometry and accessibility (Fig. 3). The anticline is a southwest-vergent, asymmetric, third-order fold developed on the limb of one of the range's main synclines. The fold is upright, largely parallel, and plunges shallowly to the northwest (Figs 3 & 4). Although the regional décollement lies near the base of the McGowan Creek Formation, other prominent décollement levels exist at Willow Creek and throughout the Lost River Range leading to widespread fold disharmony (Messina, 1993). At the level of the Scott Peak Formation, the Willow Creek anticline has a close chevron core which broadens

up-section into an open, conjugate box fold, then back towards a chevron shape at the top of the exposure (Fig. 3).

Limestones of the Scott Peak Formation are uniformly twinned but pressure solution strain is preferentially partitioned into thin biomicritic beds resulting in localized strong cleavage development. Within the Willow Creek anticline, massive biopackstone beds > 2 m in thickness are generally uncleaved, whereas thinner, sparse biomicrite beds < 0.25 m thick are moderately to strongly cleaved within the anticline (Fig. 5). Massive layers dominate the exposure and are separated from one another by either discrete bedding-parallel faults with shear fibers or more strongly cleaved, bedding-parallel deformation zones. Deformation zones contain abundant selvages and strain fringes developed at the margins of pyrite framboids and detrital grains. Cleavage forms a divergent fan over the anticline, with a mean inclination of 72° W on the western limb and 71° E on the eastern limb (Fig. 4b). In order to evaluate the relationship between structural geometry (layer shape and structural position) and décollement fold kinematics, we sampled several cleaved Scott Peak beds around the Willow Creek anticline for incremental strain analysis.

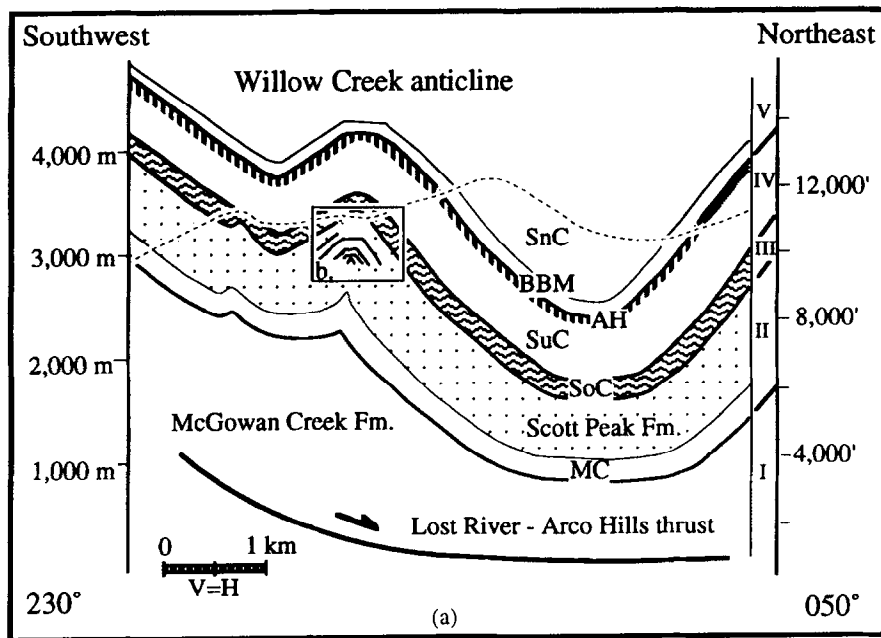


Fig. 3. (a) Interpretive cross-section of the Willow Creek structure. Solid box indicates area of photo (b), form lines shown for layers sampled in kinematic study. MC: Middle Canyon Fm., SoC: South Creek Fm., SuC: Surratt Canyon Fm., AH: Arco Hills Fm., BBM: Bluebird Mountain Fm., SnC: Snaky Canyon Fm. Lithotectonic units are defined on the basis of fold disharmony and indicated by roman numerals (I-V). (b) View south (reversed) of the Willow Creek anticline, vertical relief equals  $\sim 700$  m.

### INCREMENTAL STRAIN ANALYSIS

Antitaxial and syntaxial fibrous mineral growth occurs in strain fringes and syntaxial veins in the Scott Peak Formation at Willow Creek anticline. Antitaxial strain fringes are characterized by a difference in mineralogy between host grains and overgrowths, whereas syntaxial fibers match host mineralogy and grow with crystallographic continuity (Durney and Ramsay, 1973). During development of antitaxial strain fringes, material is added to matrix grains at the interface between the matrix and a host grain. In syntaxial strain fringes,

material is added to the host grain or at the tip of growing fibers. In this case, the host grain becomes increasingly elliptical with continued deformation. While both types of fiber growth were observed in samples from the Willow Creek anticline, antitaxial overgrowths are considerably more abundant. The antitaxial strain fringes consist of quartz fibers around nearly spherical or euhedral pyrite and calcite fibers around quartz-replaced bioclasts (Fig. 6). Syntaxial overgrowths within the rocks are composed of calcite fibers fringing carbonate bioclasts.

Deformation zones of the Willow Creek anticline contain strain fringes characterized by (1) syntaxial

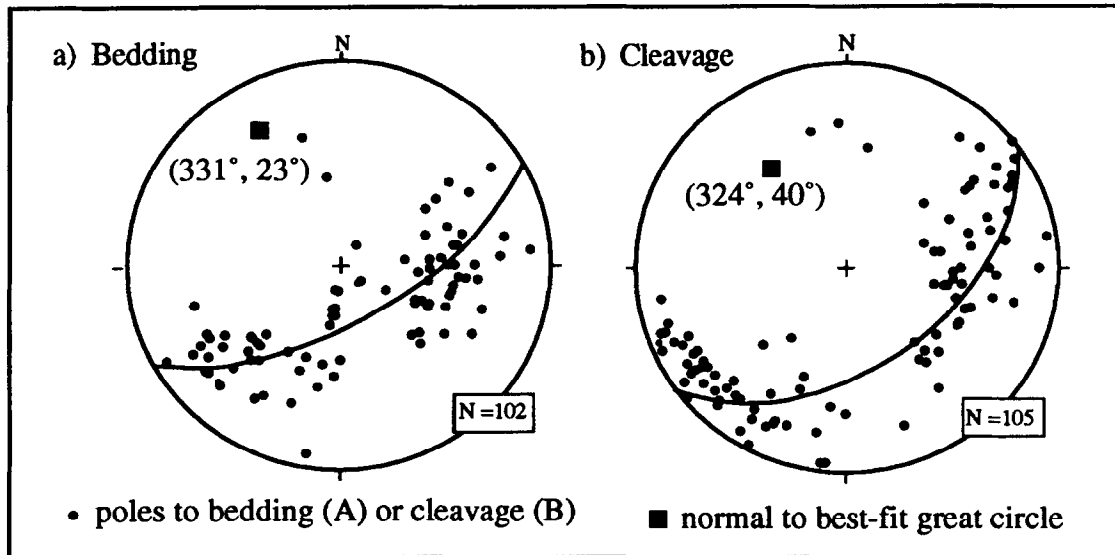


Fig. 4. Equal area lower hemisphere stereographic projections of poles to bedding (a) and poles to cleavage (b) for the Willow Creek anticline.



Fig. 5. Photograph south (reversed) of a typical Scott Peak Formation outcrop. Most samples for incremental strain analysis are from the more intensely cleaved layers.



Fig. 6. Antitaxial calcite fibers associated with a quartz-replaced bioclast host. Sample 94DA99, field of view  $\sim 1$  mm.

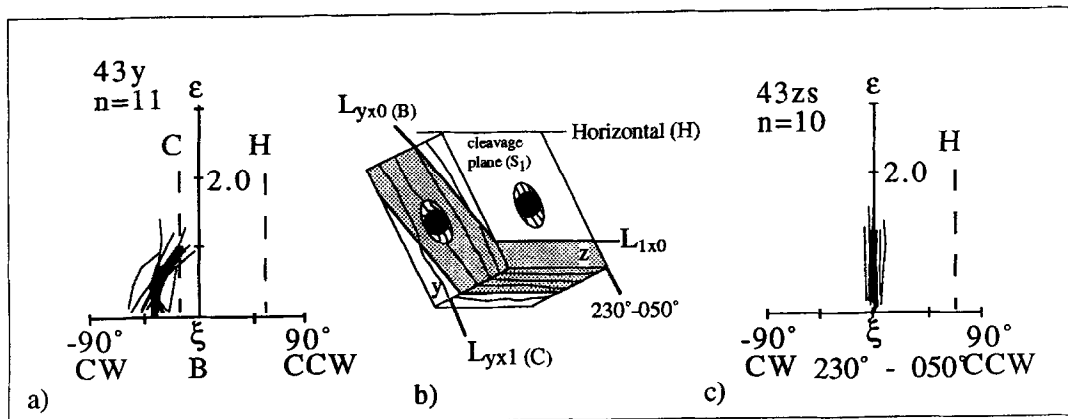


Fig. 7. Incremental strain analysis for sample 43y. (a) Cumulative incremental strain history (CISH) plot for  $XZ$  principal plane. Thin lines represent the variation of extension ( $\epsilon$ ) measured with respect to bedding ( $\xi = 0^\circ$ ) using the Durney and Ramsay (1973) 'pyrite method' for a centrally located mineral fiber within an individual strain shadow. The thick black line represents the average strain history for a thin section where  $n$  = number of measured mineral fibers. Orientations of horizontal ( $H$ ) and cleavage ( $C$ ) are indicated by the dashed lines. A counterclockwise rotation of the extension direction is positive while a clockwise rotation is negative. (b) Sketch illustrating relationship between measurement planes ( $XZ$ ,  $y$ , or profile plane, and  $XY$ ,  $z$ , or cleavage plane) and reference frames. (c) CISH for  $XY$  plane, sample 43zs, with extension plotted with respect to the regional shortening direction; ( $s$ ) indicates measurements of syntaxial strain shadows.

fibers that are in optical continuity with the host grain, (2) fibers which exhibit few deformation features such as mechanical twinning of calcite, undulatory extinction of quartz, recrystallization of quartz or calcite, or internal truncation surfaces, and (3) syntaxial and antitaxial fibers with opposing senses of curvature in the same thin section. These observations indicate that fibers are displacement-controlled and rigid, and thus should retain their primary curvature (Durney and Ramsay, 1973; Beutner and Diegel, 1985; Ellis, 1986; Spencer, 1991; Aerden, 1996). Therefore, incremental strain histories for antitaxial and syntaxial overgrowths were determined from fibers using the 'pyrite and crinoid methods' of Durney and Ramsay (1973).

Strain fringe geometry was examined in the fold profile plane (oriented orthogonal to the cleavage–bedding intersection) looking northwest parallel to the fold axis and parallel to cleavage looking down upon cleavage planes (Fig. 7). Individual mineral fibers were chosen from the center of one side of strain fringes and digitized using the trace of bedding as a reference frame. Cumulative incremental strain histories were generated for each strain fringe in a thin section. These individual histories were averaged by normalizing each strain history to the average of their end points and then averaging the curves (Clark *et al.*, 1993; Fisher and Anastasio, 1994). The dispersion of the individual curves is a reflection of the strain heterogeneity at a thin section scale, and the slope of the cumulative incremental strain curves is a measure of the external vorticity; horizontal paths represent rigid body rotations while vertical paths in horizontal samples represent coaxial deformation. The cumulative incremental strain history for a curved overgrowth is approximated by a series of small increments of pure shear separated by rigid body rotations (Elliott, 1972).

## RESULTS

Sampling for this study focused on several well-cleaved horizons which were accessible on both limb and hinge areas of the Willow Creek anticline. Approximately 150 oriented samples were collected from four horizons within the Scott Peak Formation. One third of the samples collected contained strain fringes suitable for measurement and were used to constrain the kinematics of folding. Synkinematic mineral fibers in strain fringes from cleavage-parallel thin sections are ubiquitously straight and parallel to dip throughout the Willow Creek anticline (Fig. 7). The lack of textural evidence for extension or shortening parallel to strike ( $Y$ ) and the lack of any fiber curvature in cleavage planes indicates extension; therefore, only data from  $XZ$  (fold profile) sections are presented in the kinematic analysis.

Cumulative incremental strain histories generated from the Willow Creek anticline are shown in Fig. 8 (a & b). Fibrous overgrowths from hinge or upper flat panel samples are straight or show only slight curvature ( $< 10^\circ$ ; samples 94DA99y, 94DA102y, 49ys, 50y, 51y, 83y, 84y) irrespective of a chevron or box hinge shape. Samples from the southwestern limb record clockwise reorientation of extension directions, while fibers from northeastern limb samples show consistent counterclockwise reorientations. The initial incremental extension direction of the southwestern limb was oriented at moderate angles to bedding ( $46^\circ \pm 12^\circ (1\sigma)$ ) and during deformation progressively rotated counterclockwise to shallower angles ( $29^\circ \pm 19^\circ (1\sigma)$ ). The initial incremental extension direction on the northeastern limb was also oriented at moderate angles to bedding ( $42.5^\circ \pm 16^\circ (1\sigma)$ ) but rotated clockwise to shallower angles to bedding ( $24^\circ \pm 16^\circ (1\sigma)$ ) as strain accumulated. The final incremental extension direction was moderately steep ( $66^\circ \pm 12^\circ (1\sigma)$ ) for all

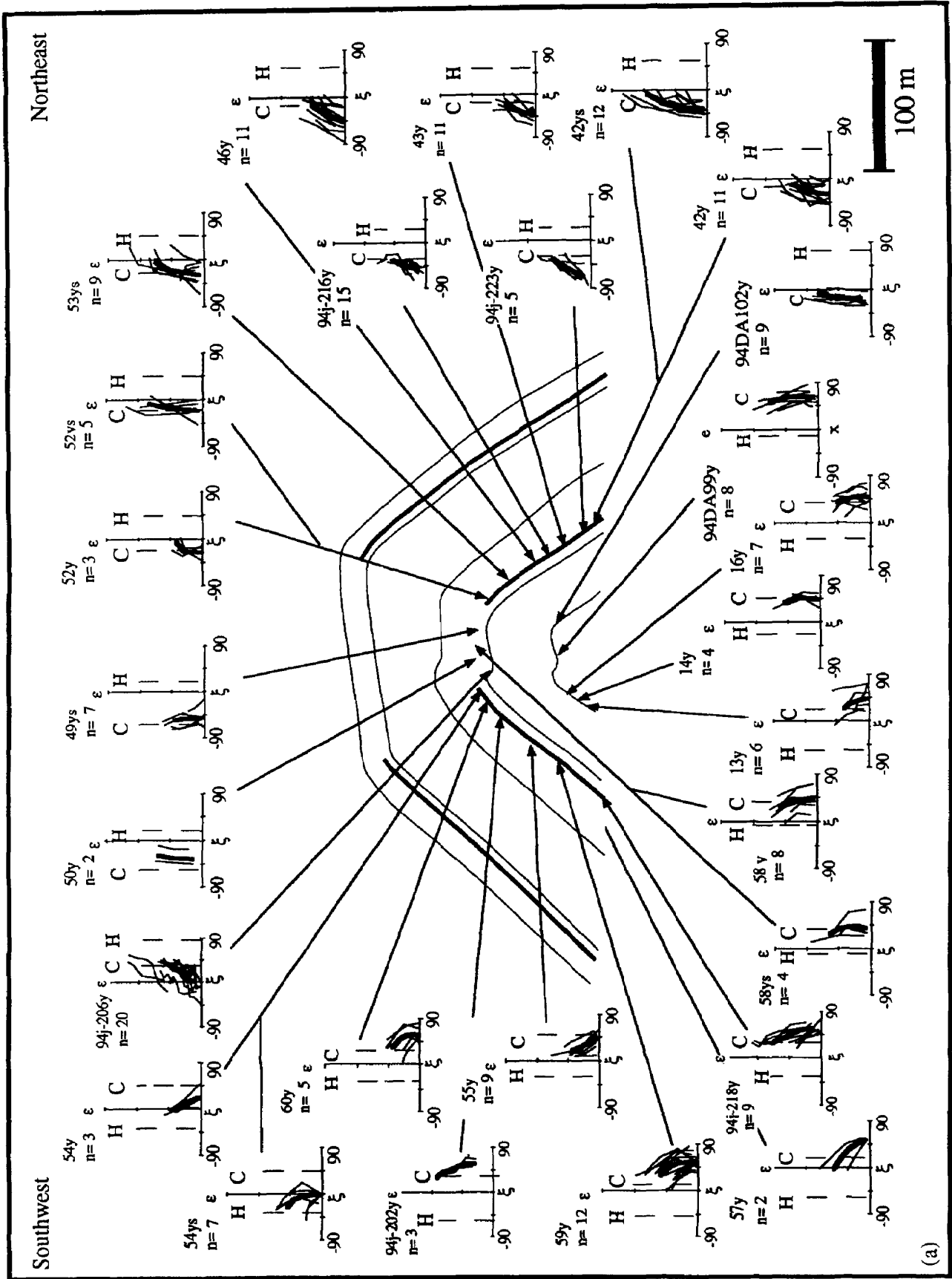


Fig. 8. (a) and (b) Cumulative incremental strain histories for XZ principal planes from Willow Creek anticline, see text and Fig. 7 caption for details.

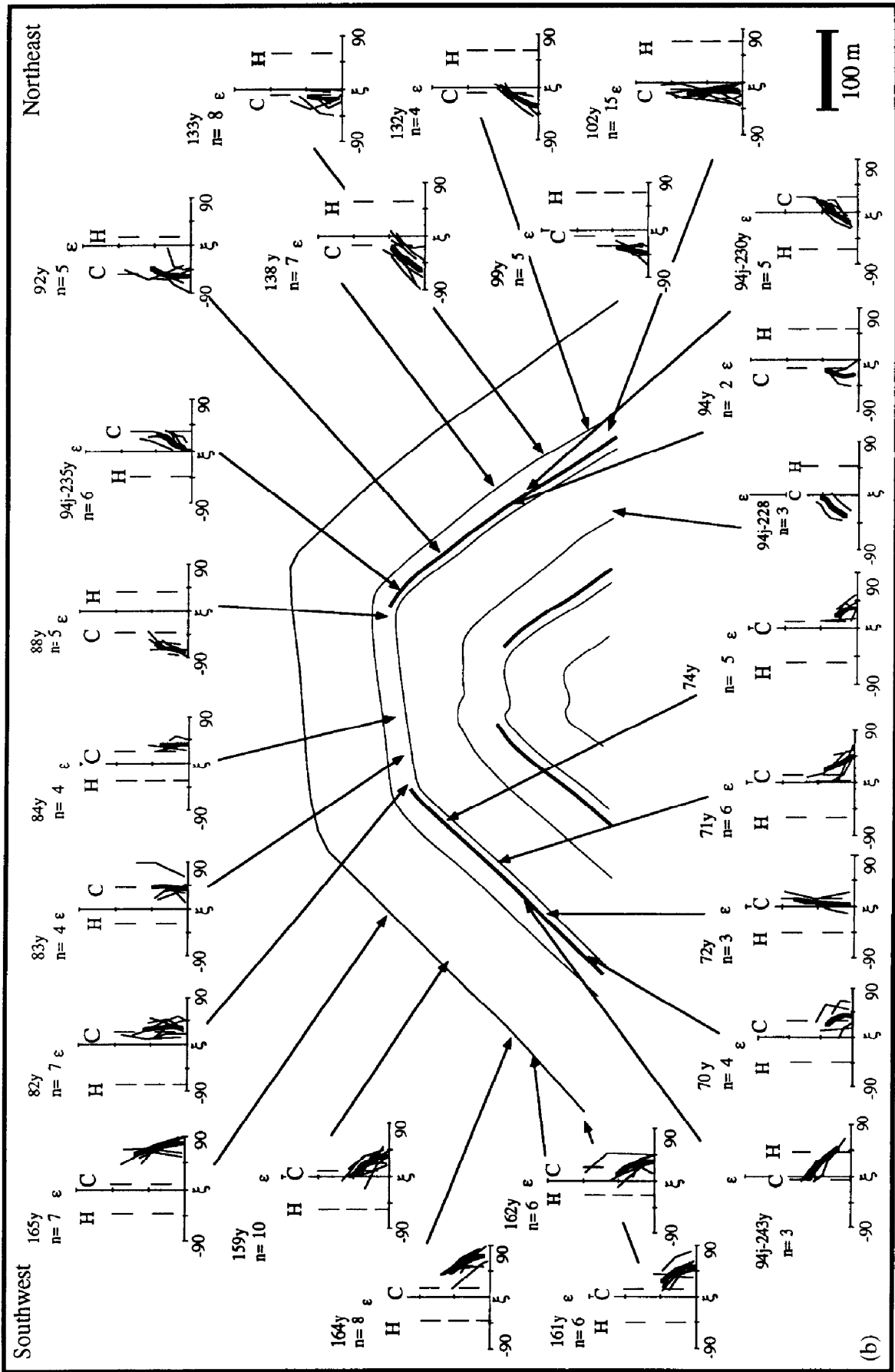


Fig. 8 (b).

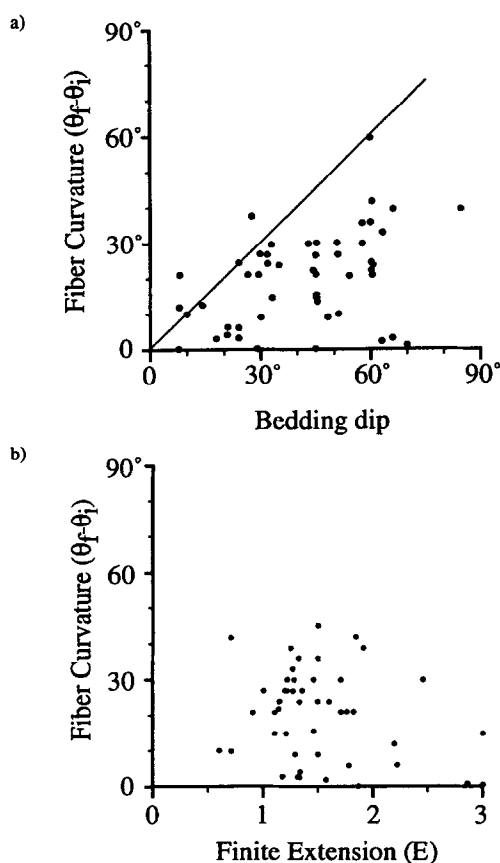


Fig. 9. (a) Plot of fiber curvature versus bedding dip for samples from Willow Creek anticline. Generally fibers record less reorientation of the principal extension direction than bedding inclination; these values are equal along the graphed line of unit slope. (b) Total extension versus fiber curvature ( $\theta_f - \theta_i$ ) for Willow Creek limb samples. See text for further discussion.

samples. The amount of fiber curvature in limb samples generally increases with limb dip, but this total external rotation is nearly always less than the bedding dip on both limbs (Fig. 9a).

Incremental strain histories from comparable structural positions around the Willow Creek anticline show the same sense of curvature, but the total curvature varies markedly between different samples (Fig. 8). For example, sample 133y shows less rotation and a shallower initial incremental extension direction with respect to bedding than nearby samples 138y and 132y. Incremental strain histories for limb samples generally have a concave down shape. Antitaxial and syntaxial pressure shadows from the same thin section record similar senses of rotation (52ys, 52y, 54ys, 54y, 58y, 58ys, 42y, 42ys), but in two of the samples, the initial incremental extension direction for syntaxial strain fringes are shallower with respect to bedding than in the antitaxial overgrowths (52ys, 52y, 54ys, 54y). Each of these syntaxial and antitaxial pairs record final incremental extension directions oriented at moderate angles to horizontal. Several steeply dipping limb samples (72y, 82y, 99y, 102y) display little fiber curvature. A few samples (42y, 46y, 58y, 59y,

138y) display considerable variation in the initial and final extension directions but record similar external rotations.

The final orientation of the finite strain ellipse determined from the strain fringes was nearly parallel to cleavage in most samples. The amount of finite elongation ( $E$ ) recorded by the fibrous overgrowths varied from 0.6 to  $>3$  (Fig. 9b). Chevron layers recorded higher strains on average in hinge areas ( $E=2.2-3.0$ ) than the horizontal panel of box folded layers ( $E=1.5-2.0$ ). All samples from the limbs recorded relatively consistent amounts of finite elongation with an average of 1.4.

## DISCUSSION

Synkinematic mineral fibers in veins and strain fringes have the potential to record the external vorticity, or the average rate of rotation of all material lines relative to an arbitrary external reference frame (e.g. bedding, cleavage, or geographic coordinates). The fiber curvature documents an external rotation that may reflect a combination of (1) spin, or rotation of the incremental extension axes relative to an external reference frame and (2) internal rotation, or rotation of early-formed fiber segments with respect to an internal reference frame (e.g. the shear plane; Fig. 10). Straight fibers will result from coaxial deformation when the spin is equal to zero or from non-coaxial deformation when the internal vorticity equals twice the spin in an opposing sense (Means *et al.*, 1980; Means, 1994).

Studies of fold kinematics are based on comparisons between measured incremental strain histories and patterns predicted for various folding mechanisms. During flexural-slip folding, interbed shear is accomplished on discrete surfaces and the deformation in the interior of beds reflects position with respect to pin lines and fold geometry. Near the hinge of an anticline, a bed may shorten or extend parallel to layering, depending on the position relative to the finite neutral surface. Fibers in pressure shadows in the outer and inner arc of the folded layer may record coaxial extension parallel and perpendicular to layering, respectively (Fisher and Anastasio, 1994). Straight limbs on the same anticline may experience an early layer-parallel shortening followed by spin through a near vertical extension direction (Wickham, 1973; Wickham and Anthony, 1977; Fisher, 1990; Fisher and Anastasio, 1994). Under these circumstances, fibers in strain fringes record stretching perpendicular to bedding initially, followed by a rotation and near-vertical extension oblique to bedding (Fig. 10). During flexural-shear folding, intrabed shear is accomplished by distributed simple shear. Fibrous strain fringes experience fiber growth oblique to bedding throughout the history of folding, but early fiber segments are rotated toward the shear (bedding) plane.

Folding could also occur by a general shear within weak layers, with a kinematic vorticity number ( $W_k$ ) that

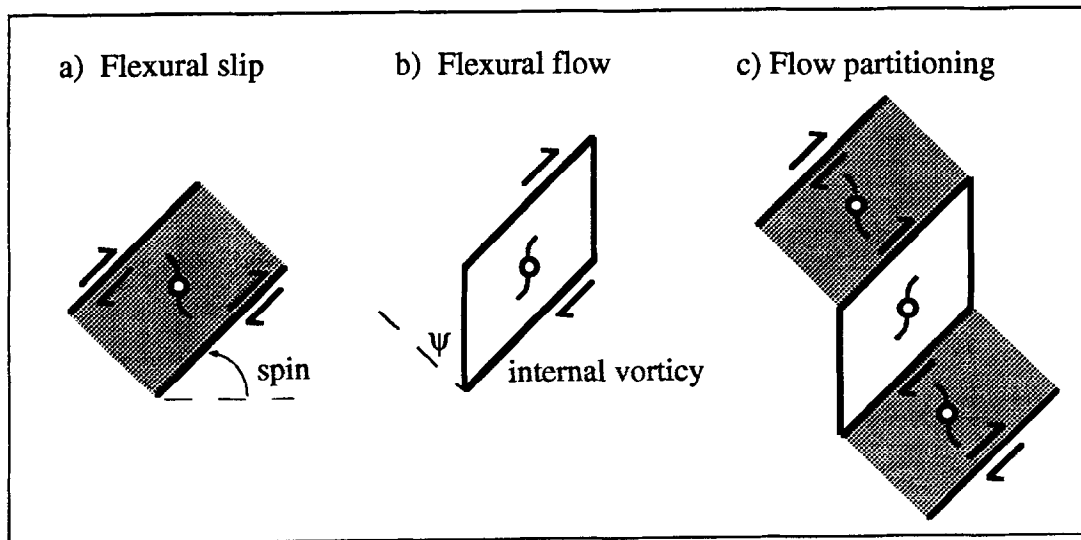


Fig. 10. Layer-parallel shear may be localized on discrete bedding-parallel faults resulting in a flexural-slip folding mechanism (left) while bed interiors deform in pure shear and record spin relative to a fixed, external extension direction. During flexural-flow folding (center), bed interiors will record distributed layer-parallel simple shearing producing an opposite sense of fiber curvature. Flow partitioning may result in kinematic partitioning between adjacent layers (right).

varies temporally and spatially and reflects the position with respect to the evolving fold geometry. For example, given that the bedding plane is a shear plane that defines the kinematic frame (i.e. an internal reference frame), a bed will deform by pure shearing ( $W_k \sim 0$ ) near the pinned hinge of a fold. On the limbs, bedding rotates during deformation, so  $W_k$  should vary during fold development.  $W_k$  would initially be  $\sim 0$  (with maximum stretching nearly perpendicular to bedding) but deformation of beds would approach simple shearing ( $W_k \sim 1$ ) as bedding planes spin into an orientation parallel to the plane of no incremental elongation. The limbs of tightening folds could experience a subsequent decrease in  $W_k$  as the bedding plane rotates towards parallelism with the maximum stretching direction. Thus, the internal vorticity related to bedding-parallel shear increases and then decreases. The more competent layers may record an early history of layer-parallel shortening followed by spin and finally, late stage interlimb tightening. In contrast, the weak layers experience an internal rotation that accompanies the spin (and with an opposite sense). The magnitude of the internal rotation depends on the thickness and spacing of weak layers. Thus, the fiber curvature in pressure shadows from weak, bedding-parallel zones reflects both the spin that occurs between the early shortening and the late limb tightening and the internal vorticity that increases and decreases with the spin but has an absolute magnitude that depends on the distribution of weak layers.

The relative importance of internal vorticity and spin in the development of fiber curvature may be easy to distinguish because the internal vorticity is of an opposite sense to the spin associated with limb rotation (Fig. 10). Thus, fibrous pressure shadows in these weak layers

could curve clockwise or counterclockwise, depending on whether the strain history defined by fiber curvature is dominated by layer-parallel shear. If the internal rotation is small, then early fiber segments are oriented at a high angle to bedding and late increments are oblique to bedding. If the internal rotation is large, early fiber segments are near-parallel to bedding and late increments are oblique to bedding (Fisher and Anastasio, 1994). The kinematics cannot be interpreted based solely on a cumulative incremental strain history without some consideration of the relative importance of spin and internal vorticity in the development of fiber curvature.

Fibrous overgrowths from the limbs of the Willow Creek anticline are curved, with samples from the southwestern limb recording counterclockwise rotation with respect to bedding, while those on the northeastern limb record progressive clockwise rotations as strain accumulated. Incremental strain histories from both limbs show final incremental extension directions that are moderately steep ( $66^\circ \pm 12^\circ$  ( $1\sigma$ )) and diverge across the anticline (Fig. 11). The final increments of extension are sub-parallel to the macroscopic cleavage which is arrayed in a divergent fan about the anticline. On each of the limbs, the external rotation recorded by fibers is consistent with the sense of expected spin for flexural-slip folding (Fig. 8). Overgrowths from limb samples are generally more curved with increasing dip which is also consistent with the rotation of bedding through a geographically fixed, moderately steep extension direction. However, for both limbs, the total external rotation is significantly less than the bedding dip (Fig. 10a). This discrepancy between the external rotation and the bedding dip cannot be explained by post-Sevier steepening of bedding, which would have steepened one limb and

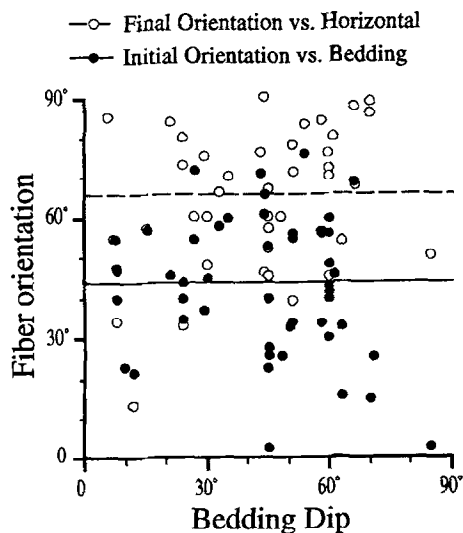


Fig. 11. Initial orientation of the direction of principal extension (filled circles) versus bedding inclination and final orientation of the extension direction (open circles) versus horizontal for Willow Creek samples. Data on the final orientation of the extension direction is consistent with synkinematic fiber curvature produced during flexural-slip folding where bed interiors record a pure shear about a fixed, moderately steep ( $\sim 66^\circ$ ), diverging extension direction. However, the initial directions are shallower than expected for flexural-slip. See text for details.

shallowed the other. In fact, the limb dip is greater than the observed fiber curvature for both limbs (Fig. 9a).

The difference between the amount of bedding dip and the amount of reorientation of the incremental extension direction may be the result of one or more of the following: (1) mineral fibers in strain fringes may be systematically deformed, (2) overgrowths may have begun developing after folding began and thereby missed the first half of limb rotation, or (3) fiber shape may be a consequence of general shear. Fiber curvature could be less than the total spin if early formed fiber segments passively rotate toward parallelism with the direction of later fiber growth (Fig. 12). Under these circumstances, fibers should show a sweep in the

extinction angle along the fiber. In a few cases, antitaxial fibers show textural evidence for deformation, but the difference in crystallographic orientation of early and late fiber segments is small ( $< 10^\circ$ ) and always significantly less than the discrepancy between the expected spin (the total limb rotation) and the fiber curvature. Samples containing both syntaxial and antitaxial strain fringes record similar initial incremental extension directions, suggesting that early fiber increments are not much deformed for either strain fringe type. While the deformation of early fiber increments during subsequent folding is possible, definitive evidence for pervasive or systematic fiber deformation is lacking in Willow Creek samples.

A second possibility is that fiber growth did not occur during the early stages of folding and that there was  $25\text{--}30^\circ$  of limb rotation on limbs prior to the onset of fiber growth. Behzadi and Dubey (1980) showed that folding in layered Plasticine models was initially accommodated by discrete sliding and only subsequently by penetrative deformation. Similarly, the Willow Creek anticline may show patterns that reflect flexural-slip with no fiber growth early in the fold history. A problem with this model is that it requires that the deformation zones record higher strain than more competent layers without any flexural flow partitioned into weak layers (Hudleston *et al.*, 1996). The lack of a positive correlation between finite extension recorded by strain fringes and fiber curvature or bedding dip (Fig. 9b) is also inconsistent with early folding on discrete faults with rigid bed interiors followed by penetratively deforming beds during subsequent limb rotation.

In the case of general shearing, fiber curvature will be less than predicted for either end-member folding mechanism. Thus, the discrepancy between the total rotation recorded by both limbs and the total external rotation recorded by fibers could be the result of internal rotation of early formed fiber segments related to layer-parallel shear that accompanied limb rotation. Bedding-parallel deformed zones within other fault-related folds

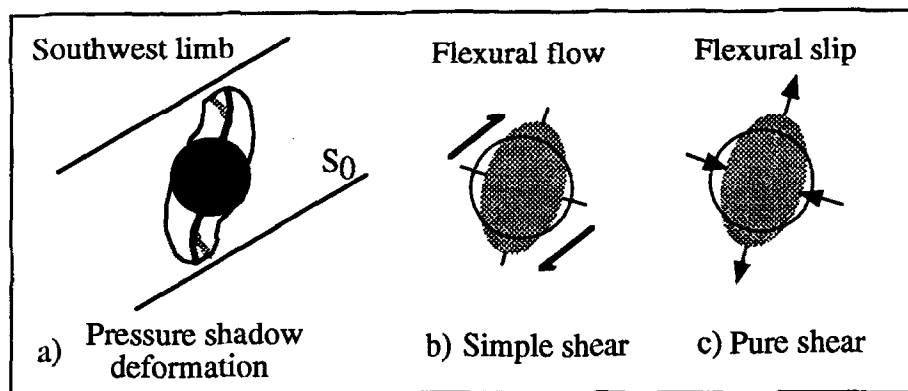


Fig. 12. (a) Strain fringe deformation. During antitaxial fiber growth, initial fiber increments (gray) may become deformed as they move away from the host. (b) Deformation with a component of hingeward bed-parallel simple shear or (c) pure shear about a fixed, steep, external extension direction (right) will result in a lessening of fiber curvature and a reduction of the angle between the initial orientation of extension with respect to bedding.

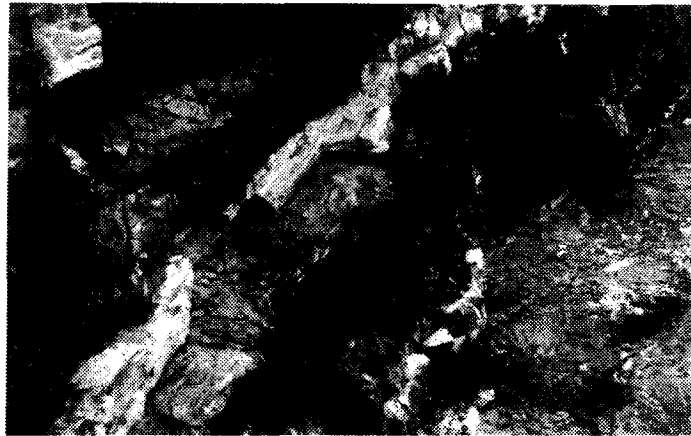


Fig. 13. An example of shear fibers on Willow Creek bedding planes (west limb, reversed); mineral accretion steps indicate relative movement of top towards the hinge of the anticline.

in the northern Lost River Range show fiber curvatures that are consistent with flexural flow (Fisher and Anastasio, 1994; Hedlund *et al.*, 1994). The strain histories from the Willow Creek anticline suggest that the elongation recorded by fibers accumulated mostly during the early and late stages of folding and that the internal vorticity and shear strain related to layer-parallel shearing did not offset the spin during limb rotation. Much of the flexural-slip along the Willow Creek anticline may have been accomplished along bedding-parallel fault surfaces with less layer-parallel shear in nearby deformed zones (Fig. 13).

Incremental strain histories from the hinge of chevron folded layers and from the flat panel of box folded layers are consistent with progressive irrotational strain ( $< 10^\circ$

rotation). Coaxial strain histories from these areas suggest that they were pinned and experienced no interbed shear during folding. Evidence of pinned hinges and a pinned flat upper panel for the Willow Creek anticline and in the adjacent anticline exposed in Buck and Mahogany Creeks (Fisher and Anastasio, 1994) suggests that décollement folding at Willow Creek occurred by progressive limb rotation, with constant limb length and limited axial surface activity (Fig. 14), similar to less deeply buried décollement folds in the Spanish Pyrenees (Holl and Anastasio, 1993; Poblet and Hardy, 1995). This situation requires a variable décollement depth within the McGowan Creek Formation (Homza and Wallace, 1995). The décollement may have initially shallowed and subsequently deepened within the Lower

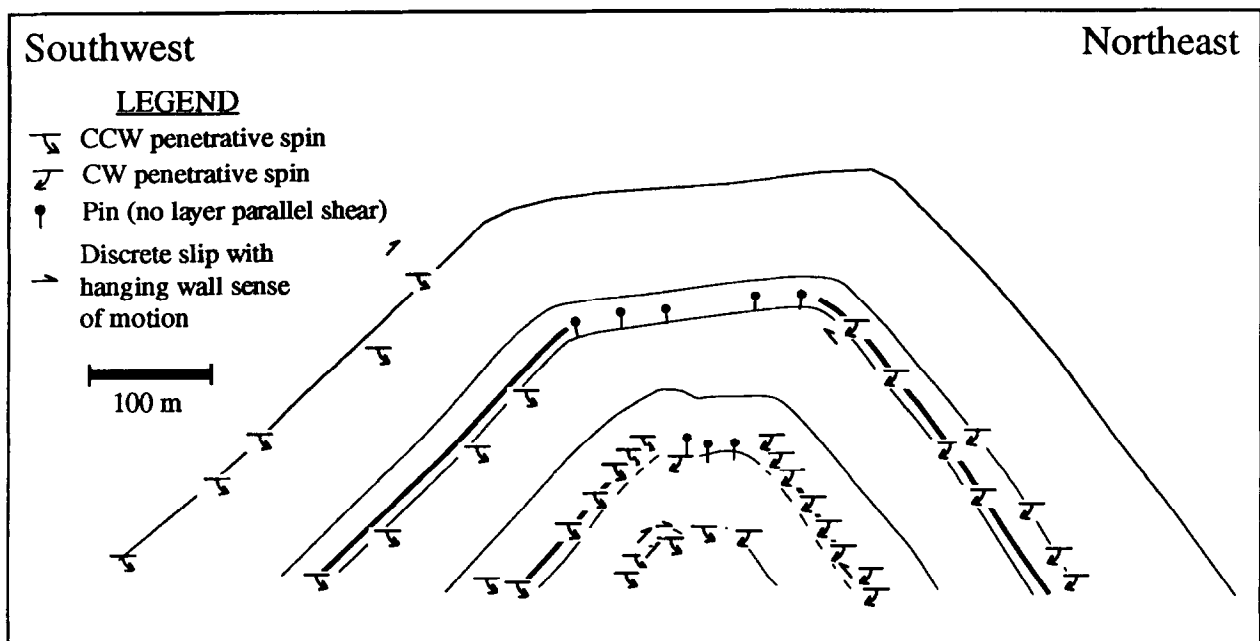


Fig. 14. Kinematic summary for the formation of Willow Creek anticline. See legend for details.

McGowan Creek Formation during development of constant limb-length décollement folds within the upper Paleozoic carbonate platform.

### CONCLUSIONS

Most folds within the northern Lost River Range plunge shallowly to the NW, are upright, and have parallel geometries with angular hinges. Sevier-age folding of the Late Paleozoic carbonate shelf was disharmonic at all scales above a décollement in the McGowan Creek Formation and resulted in 20% shortening across the range. Folding of massive (>2 m) carbonates within the Lost River Range was accommodated by the development of thin deformation zones (<0.25 m) and bedding-plane faults. Incremental strain analysis of samples from Willow Creek anticline, a large-scale décollement fold, documents plane strain deformation and folding accommodated by a combination of flexural-slip and flexural-flow about pinned hinge regions. The variations in fiber curvature present in Willow Creek samples are best explained by heterogeneous general shear in thin deformation zones which are amplified by progressive limb rotation during folding.

*Acknowledgements*—The research was supported by EAR9017334 and EAR-9405626 awarded Anastasio, EAR-9018433 awarded to Fisher, National Geographic Society grant no. 4738-92 awarded to Anastasio and Fisher, and a grant from the American Association of Petroleum Geologists awarded to Messina. Messina thanks E. R. Sherwood for field assistance and C. A. Hedlund is thanked for his early involvement in the project and for a thoughtful review of the manuscript. D. Rodgers and E. Erslev are also thanked for providing reviews of the manuscript. R. W. Allmendinger is thanked for use of his stereonet software and M. B. Clark is thanked for use of his incremental strain analysis software.

### REFERENCES

- Aerden, D. G. A. M. (1996) The pyrite-type strain fringes from Lourdes (France): indicators of Alpine thrust kinematics in the Pyrenees. *Journal of Structural Geology* **18**, 75–92.
- Allmendinger, R. W. (1990) Fold and thrust tectonics of the western United States, exclusive of the accreted terranes. In *Cordilleran Orogen: U.S.*, eds B. C. Burchfiel, P. W. Lipman and M. L. Zoback. Geological Society, America **DNAG G-3**.
- Anders, M. H., Rodgers, D. W. and Hagstrum, J. T. (1993) The growth of fault-bounded tilt blocks. *Tectonics* **12**, 1451–1459.
- Behzadi, H. and Dubey, A. K. (1980) Variation of layer slip in space and time during flexural folding. *Journal of Structural Geology* **2**, 453–457.
- Beutner, E. C. and Diegel, F. (1985) Determination of fold kinematics from syntectonic fibers in pressure shadows, Martinsburg slate, New Jersey. *American Journal of Science* **285**, 15–50.
- Boyer, S. E. (1986) Styles of folding within thrust sheets: Examples from the Appalachians and the Rocky Mountains of the USA and Canada. *Journal of Structural Geology* **8**, 325–339.
- Chamberlain, R. T. (1910) The Appalachian folds of central Pennsylvania. *Journal of Geology* **18**, 228–251.
- Clark, M. B., Fisher, D. M. and Chia-yu, L. (1993) Kinematic analysis of the Hfuehshan Range, a large-scale pop-up structure. *Tectonics* **12**, 205–217.
- Cooper, M. A. and Trayner, P. M. (1986) Thrust-surface geometry: implications for thrust-belt evolution and section balancing techniques. *Journal of Structural Geology* **8**, 305–312.
- Dahlstrom, C. D. A. (1969) Balanced cross-sections. *Canadian Journal of Earth Sciences* **6**, 743–757.
- Dahlstrom, C. D. A. (1990) Geometric constraints derived from the law of conservation of volume and applied to evolutionary models for detachment folding. *Bulletin of the American Association of Petroleum Geologists* **74**, 336–344.
- De Sitter, L. V. (1956) *Structural Geology*. McGraw-Hill, New York.
- Dixon, J. M. and Liu, S. (1992) Centrifuge modeling of the propagation of thrust faults. In *Thrust Tectonics*, ed. K. McClay, pp. 53–70. Chapman and Hall, London.
- Durney, D. W. and Ramsay, J. G. (1973) Incremental strains measured in syntectonic crystal growths. In *Gravity and Tectonics*, ed. K. A. DeJong and R. Scholten, pp. 67–96. Wiley, New York.
- Elliott, D. (1972) Deformation paths in structural geology. *Bulletin of the Geological Society, America* **83**, 2621–2638.
- Ellis, M. A. (1986) The determination of progressive deformation histories from antitaxial and syntaxial fibers. *Journal of Structural Geology* **8**, 701–709.
- Epard, J. L. and Groshong, R. H. (1993) Excess area and depth to detachment. *Bulletin of the American Association of Petroleum Geologists* **77**, 1291–1302.
- Fisher, D. M. and Anastasio, D. J. (1994) Kinematic analysis of a large-scale leading edge fold, Lost River Range, Idaho. *Journal of Structural Geology* **16**, 337–354.
- Fisher, D. M. (1990) Orientation history and rheology in slates, Kodiak and Afognak Islands, Alaska. *Journal of Structural Geology* **12**, 483–498.
- Fischer, M. P., Woodward, N. B. and Mitchell, M. M. (1992) The kinematics of break-thrust folds. *Journal of Structural Geology* **14**, 451–460.
- Hardy, S. and Poblet, J. (1994) Geometric and numerical model of progressive limb rotation in detachment folds. *Geology* **22**, 371–374.
- Hedlund, C. A., Anastasio, D. J. and Fisher, D. M. (1994) Kinematics of fault-related folding in a duplex, Lost River Range, Idaho, U.S.A.. *Journal of Structural Geology* **16**, 571–584.
- Heim, A. (1921) *Geologie der Schweiz II. Die Schweizer Alpen*. Tauchnitz, Leipzig.
- Holl, J. E. and Anastasio, D. J. (1993) Paleomagnetically derived folding rates, southern Pyrenees, Spain. *Geology* **21**, 271–274.
- Homza, X. T. and Wallace, W. K. (1995) Geometric and kinematic models for detachment folds with fixed and variable detachment depths. *Journal of Structural Geology* **17**, 575–588.
- Hudleston, P. J., Treagus, S. H. and Lan, L. (1996) Flexural flow folding: does it occur in nature? *Geology* **24**, 203–206.
- Jamison, W. (1987) Geometric analysis of fold development in overthrust terranes. *Journal of Structural Geology* **9**, 207–220.
- Jamison, W. R. (1992) Stress controls on fold thrust style. In *Thrust Tectonics*, ed. K. McClay, pp. 155–164. Chapman and Hall, London.
- Janecke, S. U., Geissman, J. W. and Bruhn, R. L. (1991) Localized rotation during Paleogene extension in east central Idaho: paleomagnetic and geologic evidence. *Tectonics* **10**, 403–432.
- Janecke, S. U. and Wilson, E. (1992) Geologic map of Borah Peak, Burnt Creek, Elkhorn Creek, and Leatherman Pass 7.5 minute quadrangles, Custer and Lemhi Counties, Idaho. Idaho Geologic Survey, Technical Report **92-5**. Moscow, Idaho.
- Mamet, B. L., Skipp, B., Sando, W. J. and Mapel, J. (1971) Biostratigraphy of upper Mississippian and associated Carboniferous rocks in south-central Idaho. *Bulletin of the American Association of Petroleum Geologists* **55**, 20–33.
- Mapel, W. J., Reed, W. H. and Smith, R. K. (1965) Geologic map and sections of the Double Springs Quadrangle, Custer and Lemhi Counties, Idaho, United States Geological Survey Map **GQ464**.
- Means, W. D. (1994) Rotational quantities in homogenous flow and the development of small-scale structure. *Journal of Structural Geology* **16**, 437–445.
- Means, W. D., Hobbs, B. E., Lister, G. S. and Williams, P. F. (1980) Vorticity and non-coaxiality in progressive deformation. *Journal of Structural Geology* **2**, 371–378.
- Messina, T. A. (1993) The geometry and kinematics of intra-thrust sheet décollement folding: Lost River Range, Idaho. Unpublished M.Sc. thesis, Lehigh University.
- Namson, J. (1981) Structure of the western Foothills Belt, Miaoli-Hsinchu Area, Taiwan: (I) southern part. *Petroleum Geology of Taiwan* **18**, 31–50.
- Poblet, J. and Hardy, S. (1995) Reverse modelling of detachment folds in the South Central Pyrenees. *Journal of Structural Geology* **17**, 1707–1724.

- Poblet, J. and McClay, K. (1996) Geometry and kinematics of single-layer detachment folds. *Bulletin of the American Association of Petroleum Geologists* **80**, 1085–1110.
- Rich, J. L. (1934) Mechanics of low-angle overthrust faulting. *Bulletin of the American Association of Petroleum Geologists* **18**, 1584–1596.
- Rodgers, D. W. and Janecke, S. U. (1992) Tertiary paleogeologic maps of the western Idaho–Wyoming–Montana thrust belt. In *Regional Geology of Eastern Idaho and Western Wyoming*, eds P. K. Link, M. A. Kuntz and L. B. Platt, *Memoirs of the Geological Society, America*, 179, 83–94.
- Ross, C. P. (1947) Geology of Borah Peak quadrangle, Idaho. *Bulletin of the Geological Society, America* **58**, 1085–1160.
- Sandberg, C. A. (1975) McGowan Creek Formation, new name for lower Mississippian flysch sequence in east-central Idaho. *United States Geological Survey Bulletin* **1405-E**, E1–E11.
- Spencer, S. (1991) The use of syntectonic fibers to determine strain estimates and deformation paths: An appraisal. *Tectonophysics* **194**, 13–34.
- Suppe, J. (1983) Geometry and kinematics of fault-bend folding. *American Journal of Science* **283**, 684–721.
- Suppe, J. and Medwedeff, D. A. (1990) Geometry and kinematics of fault-propagation folding. *Eclogae Geologicae Helveticae* **83**, 409–454.
- Suppe, J., Chou, G. T. and Hook, S. C. (1992) Rates of folding and faulting determined from growth strata. In *Thrust Tectonics*, ed. K. McClay, pp. 105–122. Chapman and Hall, London.
- Suppe, J., Sabat, F., Muñoz, J., Poblet, J., Roca, E. and Verges, J. (1997) Bed-by-bed fold growth by kink-band migration: Sant Llorenç de Morunys, eastern Pyrenees. *Journal of Structural Geology*, **19**, 443–461.
- Wickham, J. (1973) An estimate of strain increments in naturally deformed carbonate rock. *American Journal of Science* **273**, 23–47.
- Wickham, J. and Anthony, M. (1977) Strain paths and folding in carbonate rocks near Blue Ridge, central Appalachians. *Bulletin of the Geological Society, America* **88**, 920–924.
- Zapata, T. R. and Allmendinger, R. W. (1996) Growth stratal records of instantaneous and progressive limb rotation in the Pre-cordillera thrust belt and Bermejo basin, Argentina. *Tectonics* **15**, 1065–1083.